










Antidote activity of vitamin B₁₂ derivative compared with its original and aqua forms; in vitro and in vivo study

Olga A. Gromova¹  · Larissa A. Maiorova¹  · Denis S. Salnikov²  · Ivan Yu Torshin¹  · Vadim I. Demidov³ · Irina K. Tomilova³ · O. I. Koifman² · Alla G. Kalacheva³ · Tatiana E. Bogacheva³ · Elena L. Alexakhina³ · Tatiana R. Grishina³ · Andrei N. Gromov¹ · Elham Assadpour^{4,5}  · Tolulope J. Ashaolu^{6,7}  · Seid Mahdi Jafari^{8,9} 

Revised: 3 February 2025 / Accepted: 13 February 2025
© Association of Food Scientists & Technologists (India) 2025

Abstract

Vitamin B₁₂ (VB12) – essential nutrient, required for detoxication of homocysteine, support of the myelinization in neural tissue and of the hematopoiesis. Certain drugs (such as antibiotics or antituberculosis drugs) result in deep deficiency of VB12. Using VB12 and its derivatives as antidotes is a promising direction in pharmacology, that allows compensation of the toxic effects of the drugs by nutraceuticals. In the present work, interactions of isoniazid (IZ) (a toxic drug, used in the pharmacotherapy of tuberculosis) with various VB12 derivatives were studied. An in vitro study in aqueous solutions with different pH values showed that the hydrophobic derivative of VB12—heptamethyl ester of aquacyanocobyrinic acid (ACm) promoted oxidation of IZ and contributed to reducing its hepatotoxicity. The effects of ACm were compared with VB12 and aquacobalamin in a rat model of acute IZ-induced hepatitis. IZ intoxication resulted in higher levels of aspartate aminotransferase (AST). Administration of VB12 and ACm normalized AST levels; treatment with aquacobalamin or ACm normalized total protein levels in blood serum. ACm also attenuated bilirubin levels in the blood. All VB12 derivatives significantly reduced lipid peroxidation, which was increased after IZ model was reproduced. Histological analysis confirmed the protective effects of these compounds on the rats' livers, kidneys, and brains: hepatocyte damage, inflammatory cell infiltration of liver tissues, acute ischemia of the renal cortex, and structural brain damage caused by IZ were all reduced. ACm had more positive effects on the liver than the other two compounds.

Keywords Vitamin B₁₂ · Hydrophobic derivatives · Antidotes · Antioxidant effect · Isoniazid · Neuroprotection · Hepatoprotection

Introduction

Insufficient supply of group B vitamins, especially vitamin B12 (cyanocobalamin or VB12), is widespread in various populations. VB12 deficiency is especially common in people on a strict vegetarian diet (not taking special multivitamin complexes), in women of reproductive age (Oh et al. 2020), in patients receiving long-term antibacterial therapy (for example, in the treatment of tuberculosis), etc. toxic effects of the drugs can be counteracted by nutraceuticals such as VB12. A deficit vitamin B₁₂ in food or its low absorption in the stomach and intestines is associated with a severe form of hyperhomocysteinemia (Guéant et al.

2023), which leads to oxidative stress and lipid metabolism disorders, and provokes severe atherosclerosis (Haloul et al. 2020). Nutritional support with vitamin B₁₂ and folates through food supplements can significantly improve metabolism in patients with hyperhomocysteinemia. A clinical study showed that in severe hyperhomocysteinemia caused by nutritional or hereditary folate metabolism disorders cycle, deficit VB12 and folate increased cardiovascular risk and mortality (Levy et al. 2021). Supplementation with VB12 (1000 mcg/day) and folate (5000 mcg/day) for 12 weeks reduced level toxic metabolite—asymmetric dimethylarginine V plasma at patients With sharp ischemic stroke (Xia et al. 2014).

In tuberculosis, patients often have a combined deficiency of microelements, iron deficiency anemia, hypovitaminosis of group B vitamins, and a lack of antioxidants from vegetables. In a cohort study of various dietary patterns in 605

O. I. Koifman: Deceased on 31/12/2023.

Extended author information available on the last page of the article

patients with tuberculosis in China with a high risk of liver damage caused by anti-tuberculosis drugs, a negative effect of the dietary regimen "Offal meat, poultry, and vegetable oil with insufficient vegetable consumption" on the indices of cytolysis in the liver, the risk of damage, and liver dysfunction was established. Therapy with antibiotics and specific anti-tuberculosis drugs (isoniazid, metazid, larusan, streptomycin, rifampicin) negatively interferes with the metabolism of vitamins B₆ and B₁₂, and also leads to drug-induced hepatitis (Gebremicael et al. 2019; Zhang et al. 2022). In the treatment of hepatotoxic antibiotics, combined supplements of spirulina enriched in particular with VB12 are tested (Martin 2017). Correction of the diet with VB12, spirulina and beta-carotene in rats with a tuberculosis model receiving rifampicin and isoniazid led to a weakening of hepatotoxicity, inflammatory blood markers and an improvement in the immunohistochemistry of liver sections (Wang et al. 2024). Replenishment of VB12 is very important for patients suffering from tuberculosis infection. They are recommended to take additional VB12 in the form of food supplements, and if necessary, in combination with other minor micronutrients (vitamin B₆, vitamin A, beta-carotene) while maintaining sufficient consumption of meat by-products, poultry, fruits and vegetables.

Antidotes are chemicals that alter the action of a poison in the body to prevent, reverse, or mitigate the toxic effects. Examples of mechanisms by which antidotes work include competition at a receptor site, alteration of a metabolic process, engaging a counter-regulatory physiologic process, or hastening the excretion or detoxification of a toxin. The studies dealing with vitamins and their derivatives as possible antidotes are quite few. An important area of research in pharmacology and physico-chemical medicine of vitamin derivatives is the search for antidotes against targeted pharmaceuticals. Aquacobalamin (aqua form of vitamin B₁₂) is recommended as an antidote at cyanide poisoning. The studies of its derivative, diaquacobinamide, has showed that it is notably more effective than aquacobalamin (AQ) at the poisoning (Lee et al. 2016). Moreover, it could potentially serve as a methyl mercaptan (Philipopoulos et al. 2022) and hydrogen sulfide (Jiang et al. 2016) antidote.

In general, the establishment of the mechanisms for antidote action of vitamin B₁₂ (VB12) and its derivatives is an interesting and important direction in the molecular pharmacology. The known biological roles of cobalamins (including cyanocobalamin, known as VB12) and the possibility of their chemical modifications make it possible to develop new drugs. In particular, a promising area of research is the search for cobalamin/corrin antidotes (Hendry-Hofer et al. 2021), including those against intoxication with pharmacological drugs. Micro- and nanoencapsulation technologies are important for targeted delivery and modulation of the biological properties of such molecules (Gromova et al.

2021). Also, there are compounds with hydrophobic modifications of the corrin ring of VB12 – for example, aquacyanocobyrinic acid heptamethyl ester (ACm).

Earlier we have shown that ACm, VB12, and AQ can be recommended for further study as analgesics and anti-inflammatory agents (Gromova et al. 2021). The ACm, in particular, is soluble in water and a wide range of organic solvents and exhibits a biological activity (protection of the myelin sheath of neurons) under conditions of toxic stress (thiosemicarbazide) (Gromova et al. 2022). The introduction of currently registered forms of VB12 and AQ saved 50% of the lives, and the introduction of unregistered ACm saved 33% of the animals. In vitro studies were carried out to explain these important and unexpected results for ACm. Analysis of the electronic absorption spectra indicated the possibility of direct interaction of the toxic thiosemicarbazide with AQ. However, the binding constant of the substance was quite small, which did not allow for explaining the observed positive effect of AQ on reducing the toxicity of thiosemicarbazide due to this interaction. The binding constant of this toxicant to the ACm was close to zero. Therefore, the establishment of the mechanisms of the antidote action of these compounds, especially ACm, requires the involvement of additional fundamental research in vitro.

The interaction mechanisms between the studied VB12 derivatives in aqueous media and the toxicant molecules might be very complex. For example, substances with sulfur-containing functional groups (thiols, sulfites, as in thiosemicarbazide) and/or nitrogen-containing groups (amino acids, pyridine, as in thiosemicarbazide or isoniazid (IZ)) can directly interact with the cobalt nucleus of VB12 hydrophobic derivatives containing water in axial position, as axial ligands. Then, such substances will replace the water molecule and form complexes with derivatives. Such complexes can undergo further chemical transformations stimulated by the cobalt ion as a kind of catalytic center. VB12 and its derivatives, together with many other important biomolecules in supramolecular assemblies, possess an impressive variety of functional properties which are used in natural systems performing their vital functions in living organisms. Previously, we successfully encapsulated VB12 in nanoengineered polymer capsules. The formation of molecular assemblies at the interfaces is a specific feature of this class of compounds (Valkova et al. 2002, 1999, 1996a; Vu et al. 2016; Maiorova et al. 2018). Self-assembly is a key player in materials nano-architectonics (Ariga et al. 2019, 2017, 2021; Webre et al. 2018; Petrova et al. 2014; Oldacre et al. 2017; Brenner et al. 2017). Supramolecular polymers have been created using diverse self-assembly strategies wherein biomolecules are employed (Shee et al. 2020; Stulz 2017). The possibility of the self-assembly of compounds into 2D and 3D nanostructures possessing controlled properties was demonstrated (Valkova et al. 1997, 1996b; Maiorova

et al. 2015; Kharitonova et al. 2018). Similar mono- and heteromolecular nanostructures containing drugs can be prepared in vitro (Soares et al. 2018; Nowak et al. 2020; Zeytunluoglu and Arslan 2022; Ouyang et al. 2019; Moraes Profirio et al. 2018) with a subsequent introduction into the body for a therapeutic effect or form spontaneously when molecular solutions were introduced. Recently, the formation of supermolecular nanoentities (SMEs) of VB12 derivative (viz. heptabutyl ester of aquacyanocobyrinic acid, ACBuCby) have been reported, i.e., unique nanoparticles exhibiting strong non-covalent intermolecular interactions and possessing intriguing properties (Maiorova et al. 2023). Besides reproducing the functional properties of VB12 complexes with proteins in living organisms, the nanoparticles demonstrate important advantages over VB12. They are more effective in oxygen reduction/evolution reactions and in transformations into other forms (Maiorova et al. 2023). Such nanoparticles can become an alternative form of VB12. Also, the first example of the formation of nanoparticles of ACm in protein nanocarriers and neuroprotective activity in vivo of the own nanoform of the drug has been revealed (Maiorova et al. 2024).

IZ is one of the first synthetic drugs against *Mycobacterium tuberculosis* and the first line of pharmacotherapy for tuberculosis (Vilchèze and Jacobs 2019). A significant disadvantage of IZ is its high hepatotoxicity (Erwin et al. 2019). Among animals, IZ intoxication in dogs is most severe (ASPCA Animal Poison Control Center Phone 2022). In case of IZ poisoning, pyridoxine hydrochloride (vitamin B₆) is used in doses equivalent to the dose of IZ taken (~ 50 mg/kg pyridoxine intravenously) (Villar et al. 1995). The high toxicity of IZ limits its use in patients with (i) liver disease, (ii) a tendency to convulsions, and (iii) low levels of pyridoxine in the blood (because of the formation of the IZ-pyridoxine complex) (O'Connor and Isoniazid 2022). Acute IZ poisoning leads to recurrent generalized tonic-clonic seizures, severe metabolic acidosis, liver and kidney damage, hematological disorders (Sridhar et al. 2012), mitochondrial insufficiency (Zhang et al. 2021), anorexia, limb tremor, and coagulopathy (Edgar et al. 2022). By long-term treatment of pulmonary forms of tuberculosis with IZ, toxic optic neuropathy of the optic nerve (Orssaud et al. 2022), psychoses and other neuropsychiatric disorders can develop (Gomes et al. 2019).

Previously, we have shown that certain hydrophilic derivatives of VB12 can be effective oxidizers of IZ and its toxic metabolites (Tumakov et al. 2019). Therefore, it is of interest to study the interactions of the toxicant IZ with ACm. Here the influence of VB12 semi-synthetic derivative on the effects associated with taking isoniazid, an anti-tuberculosis drug, was studied. We present: (1) molecular mechanisms of interaction between ACm and IZ, taking into account the pH of the solution; (2) the results of the hepato-, neuro- and

nephroprotective effects of ACm in comparison with VB12 and AQ in a model of acute hepatitis caused by IZ in rats. The effects of IZ when interacting with various VB12 derivatives were studied in vitro (in aqueous solutions) and in vivo (in a rat model of acute IZ-induced hepatitis with biochemical and histological tests).

Materials and methods

IZ (98%, from Alfa Aesar) was used without further purification. Organic solvents were purchased from Sigma-Aldrich. Acetate (0.01 M, pH = 4.7), phosphate (0.01 M, pH = 7.2), borate (0.01 M, pH = 9.2), and carbonate (0.01 M, pH = 10.7) buffers were used to control the pH as required.

Synthesis of ACm

Dicyanocobyrinic acid heptamethyl ester was produced and purified following the known procedure (Gromova et al. 2022). The structure (Fig. 1b) of this chemical was confirmed by MALDI-TOF mass spectroscopy. ACm was prepared by adding CH₃COOH to dicyanocobyrinic acid heptamethyl ester in ethanol/water (70:30) solution to pH = 4 and then passing a stream of nitrogen through the solution for ca. 24 h, as previously described (Gromova et al. 2022).

Photophysical characterization

VB12 was characterized by electron absorption spectra recorded with Shimadzu-UV-1800 and UV – Vis Cary 60 spectrophotometers.

Animal research

The study was carried out on 50 white male rats weighing 200–300 g in accordance with “Rules of good laboratory practice” (Appendix to the order of the Ministry of Health of the Russian Federation No. 199n dated 04/01/2016) (Dale et al. 2018; Brown et al. 2017) and allowed by the local ethical committee of IvGMA. During the studies, animals were kept under standard conditions in accordance with Directive 2010/63/EU of the European Parliament and of the Council of the European Union of 22 September 2010 concerning the protection of animals used in scientific studies. Indoor air control was in compliance with environmental parameters (temperature 18–26 °C, humidity 46–65%). The rats were kept in standard plastic cages with bedding; the cages were covered with steel lattice covers with a stern recess. The floor area per animal met regulatory standards. The animals were fed in accordance with Directive 2010/63/EU. The animals were given water ad libitum. The water was purified and normalized

for organoleptic properties in terms of pH, dry residue, reducing substances, carbon dioxide, nitrates and nitrites, ammonia, chlorides, sulfates, calcium and heavy metals in standard drinkers with steel spout lids.

Animals were divided into 5 groups: the 1st group (n = 10)—intact control; in the 2nd, 3rd, 4th and 5th groups of animals, the model of acute hepatitis was reproduced by intragastric administration of IZ hepatotoxin at a dose of 540 mg/kg body weight per day for 6 days (Couto and Cates 2019); the 3rd group of animals (n = 10) was intramuscularly injected with a solution of 0.5 mg VB12/ml at a dose of 60 µg/kg of animal weight per day simultaneously with IZ for 6 days and then another 10 days (registration number P No. 015993/01, OJSC "Borisovskiy Factory of Medical Preparations", Republic of Belarus); animals of the 4th group were injected with AQ at a dose of 60 µg/kg body weight per day intramuscularly (according to the same scheme as in group 3); in the 5th group of rats (n = 10), ACm in water was administered intramuscularly (according to the same scheme as in group 3) at a dose of 60 µg/kg animal weight per day.

On the 17th day of the study, blood was taken for biochemical studies and sectional material of the liver, kidneys, and brain was taken for histopathological examination. Aspartate aminotransferase (AST) and alanine aminotransferase (ALT) activity, levels of total protein, direct and total bilirubin (using Olvex standard kits), and malondialdehyde (MDA) were determined in the blood by the Jagi method (Morris et al. 2022). In the comparison groups, the process intensity of lipid peroxidation (LPO) in blood serum was determined by the method of induced chemiluminescence. Statistical data processing was carried out using the Statistica-10 program and Excel spreadsheet packages; the differences were evaluated using Mann–Whitney U-test at the upper level of significance $P < 0.05$.

Histological analysis

On the 17th day, the tissue sections of brain were prepared and fixed in 10% neutral formalin solution; one day later, the area of the precentral gyrus of the forebrain, cerebellum, and brain stem were isolated using frontal incisions. After evisceration, the liver and kidneys were fixed in a 10% neutral formalin solution; after 1 day, the organs were dissected, fragments of the right and left lobes of the liver, cortical sections of the right and left kidneys were isolated and re-fixed. After the secondary fixation and washing of the material, the dehydration of the tissues of the brain, liver and kidneys was carried out using 99% isopropyl alcohol. Subsequently, tissue samples were embedded in paraffin. Histological Sections 5–6 µm thick were made on a sledge microtome "Microm" and then stained with hematoxylin and eosin. Duplicate sections of the liver and kidneys were stained with Schiff's reagent, the brain

with toluidine blue according to the Nissl method. The assessment of pathological changes in the organs of rats when modeling toxic damage took into account the degree of circulatory disorders, the characteristics of the inflammatory response, and structural changes in parenchymal elements. Microphotographs were obtained using a microscope "Micros" MS-200 and a digital eyepiece camera DCM 900. The degree of pathological changes in each photo was estimated by experts in a 1–5 points score (5 – most pronounced histological damage, 1 – no histological damage). The statistical difference in scores between the groups was estimated by Mann–Whitney U test as significance level of $P < 0.05$.

Results and discussion

Interaction of ACm with isoniazid in aqueous media (in vitro results)

Compared to VB12, in the structure of ACm, there is no nucleotide base, and seven amide side chains are replaced by the ester groups (Fig. 1a). It was found that ACm can act as an effective oxidizer of IZ. During the reaction, Co^{3+} ion of ACm is reduced to Co^{2+} . Figure 1a shows the spectrum changes corresponding to this process. A typical kinetic curve for this reaction is shown in Fig. 1b.

It has been established that the kinetic curve can be well linearized in the coordinates " $\ln(A_{\infty} - A)$ —time", which indicates the first order of the reaction (estimated by ACm). The observed ACm recovery rate constant *versus* IZ concentration (Fig. 2a) shows that the value of reduction rate constant for ACm increases linearly with higher levels of IZ. Therefore, the order for IZ is equal to one, *i.e.* the reaction rate is related to the reactant concentrations as follows (Eq. 1):

$$r = k \times [\text{ACm}]_0 \times [\text{IZ}]_0 \quad (1)$$

where $[\text{ACm}]_0$ is the total concentration of ACm and $[\text{IZ}]_0$ is the total concentration of isoniazid (in an aqueous solution).

It was found that the spectra of the initial and IZ-reduced ACm reactions with IZ do not change in the pH range from 3.2 to 8.5. But at higher pH values, the rate of reduction of ACm with IZ increases (Fig. 2b). IZ has acid–base properties and exists in solution in four forms with $\text{pK}_{\text{a}1} = 1.99$, $\text{pK}_{\text{a}2} = 3.67$, $\text{pK}_{\text{a}3} = 10.89$ (Fig. 3). In an acidic medium, protonation of the nitrogen atoms of the pyridine ($\text{pK}_{\text{a}1}$) and hydrazide ($\text{pK}_{\text{a}2}$) fragments is possible; in an alkaline medium, deprotonation of one nitrogen atom in the hydrazide fragment ($\text{pK}_{\text{a}3}$) can occur.

ACm transforms into its hydroxo form only in an alkaline medium (at $\text{pH} > 10$). Since an increase in the reduction rate of ACm observed at a significantly lower pH, the data obtained can be explained by the participation of both

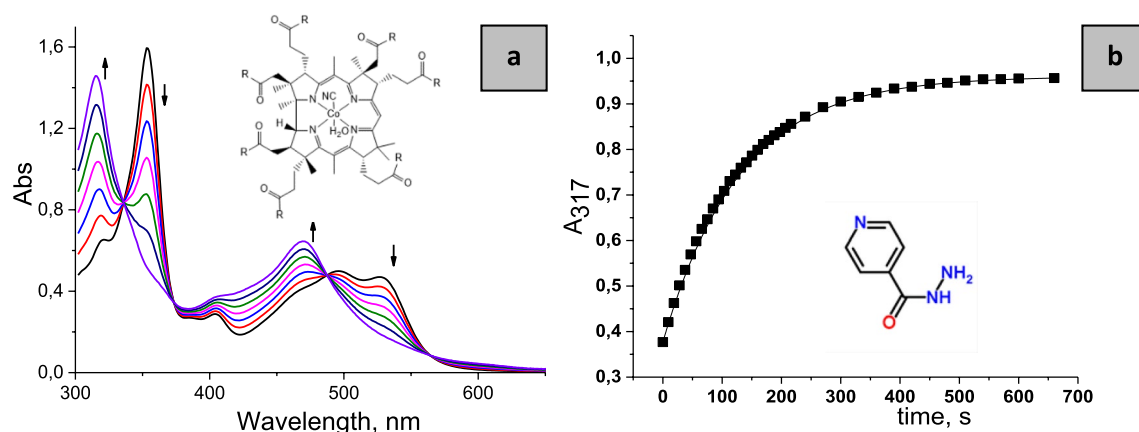


Fig. 1 **a** Spectral changes for the interaction of IZ with ACm in water under anaerobic conditions. **b** Kinetic curve for the reduction of Co^{3+} to Co^{2+} in ACm with IZ within aqueous solution. $[\text{ACm}]_0 = 5 \times 10^{-5} \text{ M}$; $[\text{IZ}] = 1 \times 10^{-2} \text{ M}$; $\text{pH} = 7.4$; 25°C . The inserts show aquacyanocobyrinic acid heptamethyl ester (ACm), $\text{R} = \text{OCH}_3$ (**a**) and IZ (**b**)

protonated and deprotonated forms of IZ in the process under study. The rate increase also shows that the deprotonated forms of IZ are stronger reducing agents. According to the pK_a values of IZ, at physiological pH, it should be in a neutral form. Our data show that at that pH value, the oxidation of IZ by ACm does proceed. Thus, at a pH close to physiological, the ACm oxidizes IZ. The reaction products, similarly to what was shown in our previous work for cobinamide (Tumakov et al. 2019), are the reduced derivative of ACm containing Co^{2+} and the oxidation products of IZ: *i.e.*, isonicotinic acid, isonicotinamide, and pyridine-4-carboxaldehyde, which do not exhibit hepatotoxic properties. The presence of isonicotinic acid in the reaction products suggests that ACm can oxidize the radical forms of IZ, which are responsible for its hepatotoxicity.

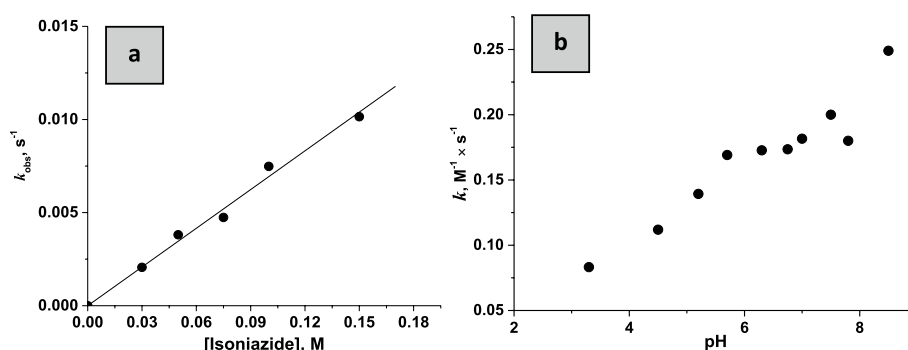
The results of acute isoniazid poisoning in rats

Preliminary experiments with IZ showed that when it was administered at a dose of LD_{50} , intoxication occurred no later than the first day from the moment of administration; then the animals gradually recovered from the state of

visually determined intoxication, and there was no lethality at later periods of observation. Repeated administration of IZ in LD_{50} dose after 24 h to rats (acute poisoning) resulted in 100% lethality. Following the literature, daily administration of IZ at a dose of 600 mg/kg ($1/2$ of LD_{50}) leads to a 20% lethality of rats only by the end of the first week of administration (on days 6–7 of administration); and only by the end of 3 weeks, the mortality can reach 100%. This phenomenon can be regarded as a true sign of the development of tolerance in rats to IZ, since over the entire period of the experiment, animals can withstand exposure to 10 LD_{50} doses of IZ (Badrinath et al. 2022).

The introduction of a high dose of IZ for 6 days led to significant liver damage: when compared with intact control (group 1), in animals of the 2nd group (which was subsequently used as the main comparison group), a significant increase in the level of blood AST (from 0.36 to 0.73 mM/h/l) and direct bilirubin (from 8.5 to 18.4 $\mu\text{M/l}$) was found. In addition, there was a decrease in the levels of total serum protein (from 56.2 to 45.6 g/l), which corresponds to a decrease in the protein-synthetic function of the liver. A well-known feature of the IZ model of hepatotoxicity

Fig. 2 **a** Rate constant of ACm reduction by IZ versus its concentration (conditions identical to those presented in Fig. 1). **b** Rate constant of ACm reduction by IZ versus pH. $[\text{ACm}]_0 = 5 \times 10^{-5} \text{ M}$, 25°C



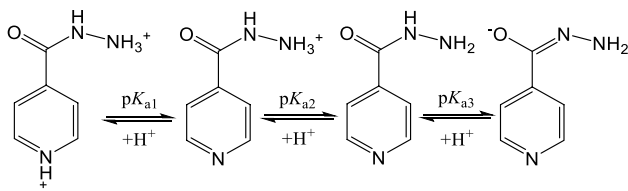


Fig. 3 Acid–base properties of isoniazid

is that there is no significant increase in malondialdehyde (MDA) levels in liver injury. Indeed, there was no significant changes in MDA levels when the model was reproduced (Table 1).

These biochemical parameters (Table 1) reflect the functional state of the liver. The levels of AST and ALT in the blood are enzymes-indicators of cytolysis (primarily, of hepatocytes). Enzymatic AST and ALT are present in significant amounts in the liver and kidneys and, therefore, their concentrations in the blood are normally low. The marker of excretory and antitoxic function of the liver is bilirubin, one of the intermediate products of hemoglobin breakdown occurring in hepatocytes (Fig. 4). MDA is formed during the degradation of fats and is a marker of oxidative stress. During the cytolysis of hepatocytes, losses of MDA, bilirubin, AST, and ALT enzymes occur, and the levels of these biochemical markers in the blood increase. Changes in the level of total protein are a sign of a gross pathology of the liver and a violation of its synthetic function. According to Mann–Whitney U-test, the reproduction of the IZ model led to a significant increase of AST levels in blood. Cyancobalamin application resulted in a significant decrease of AST ($P < 0.05$). Reproduction of the IZ model led to a significant decrease of total protein and application of AcM resulted in an increase of total protein towards the original levels ($P < 0.05$).

Changes in markers of liver and kidney function were confirmed by the results of histological analysis (Fig. 5). In intact animals (group 1), the microscopic image of the

liver tissue corresponded to the norm in all tissue samples. Within a single hepatic lobule, while maintaining histoarchitectonics, uniform perfusion of sinusoids was observed both in the central and periportal zones of the lobule. Hepatocytes had a normal configuration and uniform coloring with a correct distribution of ultrastructures in the cytoplasm (Fig. 5A). There were single lymphocytes in the stroma of the portal tracts (Fig. 5B). The study of the cortical zone of the kidneys showed the normal structure of the glomeruli with a physiological level of perfusion and free mesangial space. Nephrocytes within the convoluted proximal and distal tubules were also undamaged (Fig. 5C). The brain of rats in the control group had a normal level of perfusion without signs of aggregation of erythrocytes in the capillaries and swelling of the nervous tissue; the neurons were characterized by a normal shape and size with clear contours of the nuclei. Nissl lumps were evenly distributed in the cytoplasm of pyramidal neurons in the forebrain cortex (Fig. 5D).

When reproducing the IZ model (group 2), negative changes in the liver tissue were revealed in all of the relevant samples. Against the background of anemia in the central veins and sinusoids, widespread vacuolar dystrophy of hepatocytes, intracellular cholestasis, and discomplexation of the hepatic beams in the central zone of the hepatic lobules were noted (Fig. 5F). In the 1st, 2nd and 4th samples, there was focal necrosis of hepatocytes (Fig. 5E). Pronounced lymphohistiocytic infiltration of the stroma of the portal tracts with spread to the stroma of the sinusoids; eosinophils were present in the inflammatory infiltrate (Fig. 5I). When examining the kidneys, anemia of the glomeruli was noted against the background of spasm in the interlobular arteries (Fig. 5J), an accumulation of a protein substance in the mesangial space. Nephrocytes of the proximal convoluted tubules underwent vacuolar degeneration, and PAS-negative masses were noted in the lumens of the tubules (Fig. 5G). In the brain, against the background of spasm in small-caliber arteries, there was a pronounced

Table 1 Biochemical parameters of blood serum in the comparison groups

Group No	Observation groups	Biochemical indicators				
		AST (mM/h/l)	ALT (mM/h/l)	Total serum protein (g/l)	MDA (nM/ml)	Bilirubin direct (μM/l)
1	Control intact	0.36 ± 0.17	0.45 ± 0.10	56.2 ± 3.1	3.91 ± 0.43	8.5 ± 4.5
2	IZ, control	0.73 ± 0.13^a	0.58 ± 0.33	45.6 ± 3.4^a	4.72 ± 1.34	18.4 ± 6.3^a
3	IZ + VB12	0.58 ± 0.05^b	0.37 ± 0.12	47.6 ± 2.8	4.22 ± 0.93	16.0 ± 7.8
4	IZ + AQ	0.64 ± 0.13	0.39 ± 0.13	49.0 ± 1.2^b	4.13 ± 0.86	15.0 ± 7.6
5	IZ + ACm	0.61 ± 0.10^b	0.42 ± 0.11	$53.8 \pm 1.5^{b,c}$	4.13 ± 0.54	$9.7 \pm 5.1^{b,c}$

Note: Data are in the format of mean \pm SD (standard deviation). Significant differences were noted: ^abetween intact (group 1) and model (group 2); ^bbetween the control group (group 2, IZ) and comparison groups (3, 4, 5); ^cbetween VB12 (group 3) and groups 4, 5 (Mann–Whitney test); $P < 0.05$

ACm aquacyanocobyrinic acid heptamethyl ester

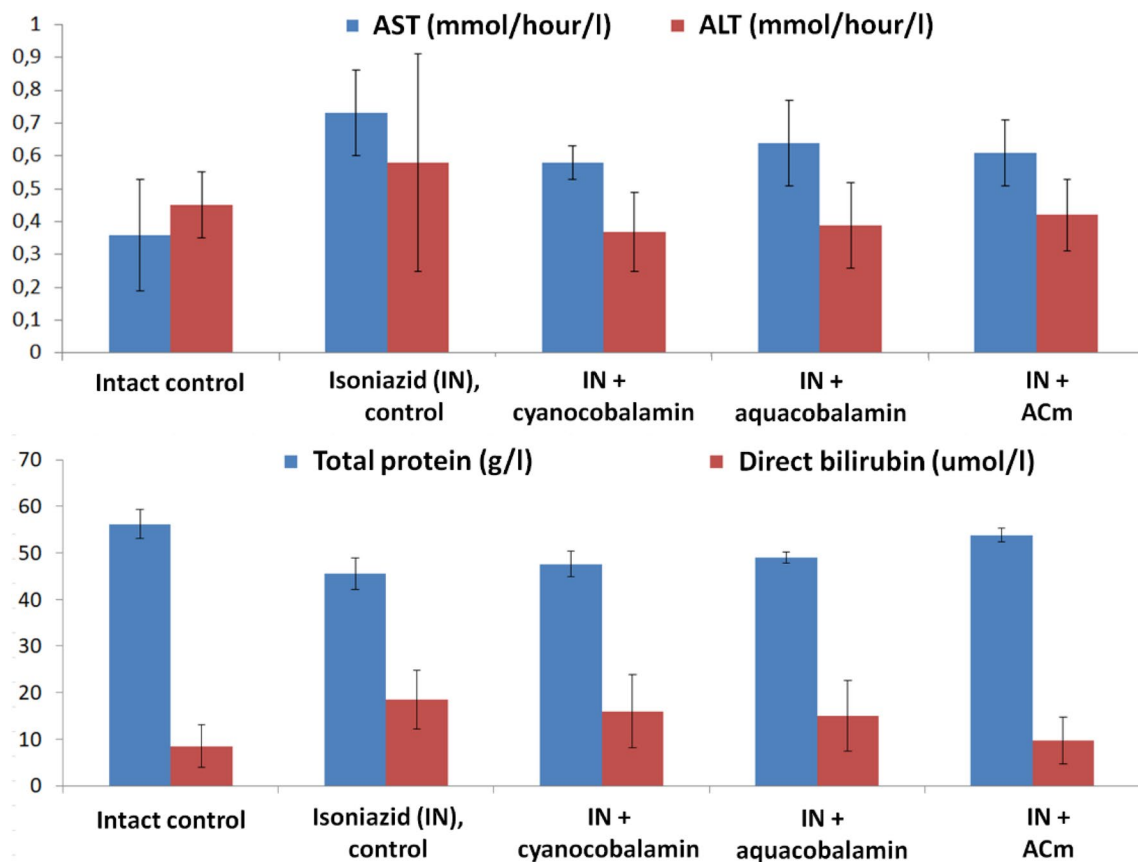


Fig. 4 Changes in biochemical markers of liver and kidney function with the use of VB12 derivatives

plethora of pial and intracerebral veins, stasis of erythrocytes in capillaries, perivascular and pericellular edema of the nervous tissue (Fig. 5K). There were small focal diapedetic hemorrhages in the cortex of the forebrain hemispheres. Changes in the pyramidal neurons of the forebrain and piriform neurons of the cerebellum were focal in nature with an ischemic type of damage. Pycnosis was observed along with hyperchromia of the cytoplasm in cortical neurons with axon swelling (Fig. 5H); similar changes were found in the cerebellum in single pear-shaped neurons. Irreversible changes in neurons, accompanied by plasmorhexis and activation of the neurophagic reaction of glial cells, were found in the 1st and 5th samples (Fig. 5L). The integral expert score of histological damage was 3.2 ± 1.5 for IZ model and 1.3 ± 0.7 for intact group which was significant according to the Mann–Whitney U-test ($P < 0.05$).

In general, the toxic effects of IZ had morphological confirmation. In the liver, there was ischemia of the centers of the lobules, subtotal protein (vacuole) dystrophy of hepatocytes (which corresponds to a decrease in the levels of total protein in a biochemical blood test, Table 1), impaired conjugation of bilirubin (with an increase in the level of direct bilirubin in the blood, Table 1), and inflammatory

cell infiltration stroma of the liver with the presence of eosinophils in the infiltrate (a sign of drug-induced hepatitis). In the kidneys, intoxication with IZ was accompanied by severe anemia of the cortex, development of widespread protein dystrophy of nephrocytes in the proximal convoluted tubules, damage to the glomerular filter with excessive filtration of protein compounds (also contributing to the development of hypoproteinemia, Table 1). In the brain, IZ stimulated circulatory disorders (mainly in the microcirculatory bed) with the development of moderately pronounced edema of the nervous tissue and with focal (mostly reversible) damage to the neurons of the cortex in the forebrain and cerebellum.

Biochemical effects of the studied compounds

The three VB12 derivatives showed significant differences in the profile of action on the studied biochemical markers. In the 3rd (VB12) and 5th (ACm) groups, a significant decrease in AST levels was noted compared with the IZ-only control (from 0.73 to 0.58...0.61 mM/h/l, Table 1). In the 4th (AQ) and 5th (ACm) groups, the content of total protein in the blood serum increased significantly compared with the

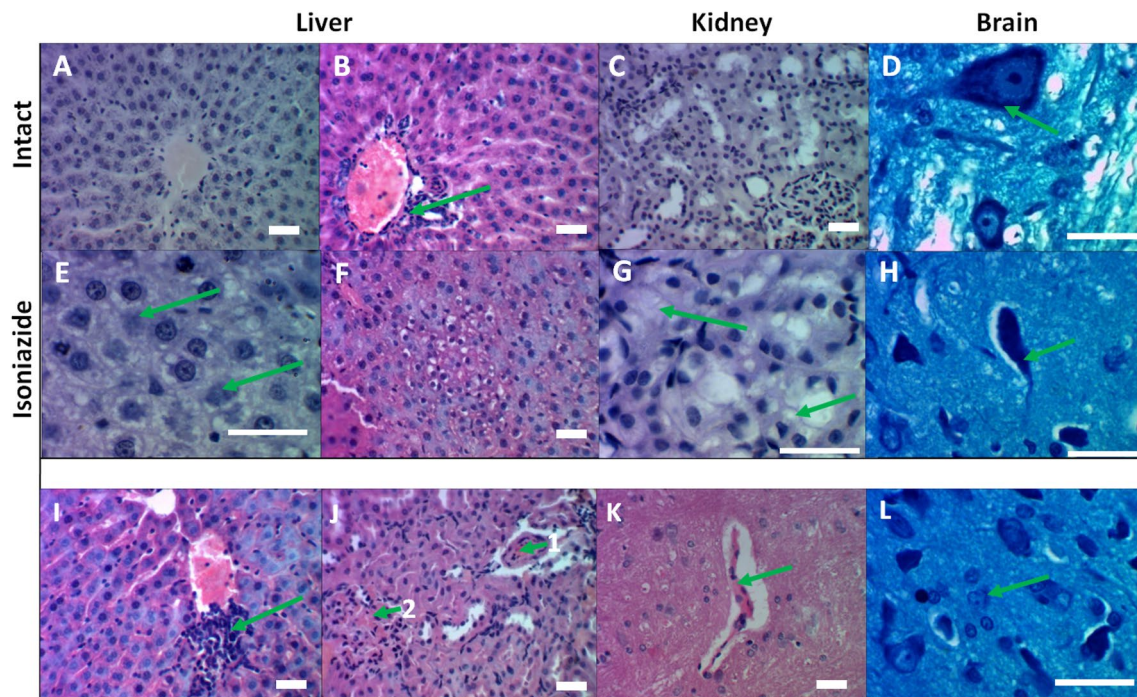


Fig. 5 Histological images of the liver, kidneys and brain in the reproduction of the model of IZ hepatotoxicity. The intact control (A–D) and the IZ model (E–L). Staining with PAS reaction (A, C, E, G), hematoxylin and eosin (B, F, I, J, K), toluidine blue according to Nissl (D, H, L). Magnification $\times 480$ (A, B, C, F, I, J, K) and $\times 1200$ (D, E, G, H, L), scale bar corresponds to 100 μm . **A** The structure of an unchanged hepatic lobule with a trabecular arrangement of hepatocytes. **B** Single lymphocytes in the stroma of the portal tract against the background of plethora of the portal vein. **C** The renal glomerulus has a capsule lumen and a free mesangium, tubular epithelial cells with a homogeneous color of the cytoplasm. **D** A pyrami-

dal neuron of a habitual configuration with a uniform distribution of Nissl clumps in the cytoplasm. **E** Vacuolar dystrophy, focal necrosis of hepatocytes in the stage of cytolysis. **F** Vacuolar degeneration of hepatocytes with impaired histoarchitectonics of the hepatic lobule. **G** Vacuolar degeneration of nephrocytes of the proximal convoluted tubules. **H** Pycnomorphic pyramidal neuron with swollen axon. **I** Lymphohistiocytic infiltrate with single eosinophils of the periportal zone. **J** Spasm of the interlobular artery, stromal edema (1), eosinophilic masses in the mesangium of the glomerulus (2). **K** Hemostasis in the capillary, perivascular and pericellular edema of the nervous tissue. **L** The reaction of microglia in the area of the dead neuron

IZ control, which indicates a possible improvement in the protein-synthetic function of the liver. The introduction of ACm led to the normalization of the AST and protein levels in the blood, as well as to the normalization of the direct bilirubin level in the blood (decrease from 18.4 to 9.7 $\mu\text{M/l}$).

The intensity results of the process of LPO by the chemiluminescence method confirmed the conclusions made based on the analysis of the other biochemical blood markers. Indicators for assessing LPO included I_{max} (maximum intensity, which reflects the potential ability of a biological object to free radical oxidation) and S (the so-called "light sum", reflects the content of RO_2 radicals corresponding to the termination of the free radical oxidation chain). In acute hepatitis caused by IZ, there was a significant increase in free radical oxidation (S, $S_1\text{max}$, α , Z, $Z_1\text{max}$) compared with intact control, while the values of tg_2 and Dec did not change significantly (Table 2).

Changes in the values of LPO parameters were more pronounced in relation to the action of the studied molecules than the previously described biochemical parameters. In

particular, all the three compounds contributed to a significant decrease in the values of LPO, which increased when playing the IZ model (S, $S_1\text{max}$, α , Z, $Z_1\text{max}$), which indicates the antioxidant activity of VB12 derivatives (Table 2). At the same time, in the 5th group (ACm), there was a more pronounced decrease in the values of S and $S_1\text{max}$ compared to group 3 (VB12). Thus, the studied compounds reduced LPO caused by IZ and increased the body's antioxidant resource.

Histological results of VB12 derivatives against isoniazid intoxication

When VB12 was taken by animals in which the IZ intoxication was reproduced, moderately pronounced plethora of portal veins was noted in the samples of liver tissue with anemia of the central veins and sinusoids along with moderately pronounced lymphohistiocytic infiltration of the portal tract stroma with the presence of single eosinophils in the infiltrate (Fig. 6A). Damage to hepatocytes was observed in

Table 2 Intensity indicators of the lipid peroxidation process in blood plasma in the studied groups

Group No	Groups	Indicators							
		I_{\max} , mV	S, mV•sec	S_1 max, mV•sec	α	Z, sec	Z_1 max, sec	tg_2 , mV/sec	Dec
1	Control intact	53.6 ± 6.3	1783 ± 197	733 ± 134	0.25 ± 0.06	14.8 ± 3.8	13.2 ± 4.1	-14.4 ± 3.1	-0.54 ± 0.47
2	IZ	72.6 ± 12.1^a	773 ± 136^a	1723 ± 436^a	0.41 ± 0.10^a	24.8 ± 6.0^a	23.9 ± 6.1^a	-13.5 ± 3.8	-0.27 ± 0.12
3	IZ + VB12	86.0 ± 15.2	1293 ± 128^b	1233 ± 124^b	0.26 ± 0.05^b	15.4 ± 2.7^b	14.7 ± 2.7^b	-18.9 ± 6.3	-0.36 ± 0.10
4	IZ + AQ	83.0 ± 25	1199 ± 288^b	1136 ± 278^b	0.25 ± 0.05^b	14.8 ± 3.0^b	14.1 ± 3.0^b	-19.5 ± 7.7	-0.39 ± 0.17
5	IZ + ACm	76.0 ± 22.4	$1133 \pm 134^{b,c}$	$1081 \pm 126^{b,c}$	0.26 ± 0.08^b	15.9 ± 4.7^b	15.2 ± 4.7^b	-17.7 ± 6.4	-0.37 ± 0.12

Data are in the format of mean \pm SD (standard deviation). Significant differences were noted: ^abetween intact (group 1) and model (group 2); ^bbetween the control group (group 2, IZ) and comparison groups (3, 4, 5); ^cbetween VB12 (group 3) and groups 4, 5 (Mann–Whitney test); $P < 0.05$

ACm aquacyanocobyrinic acid heptamethyl ester

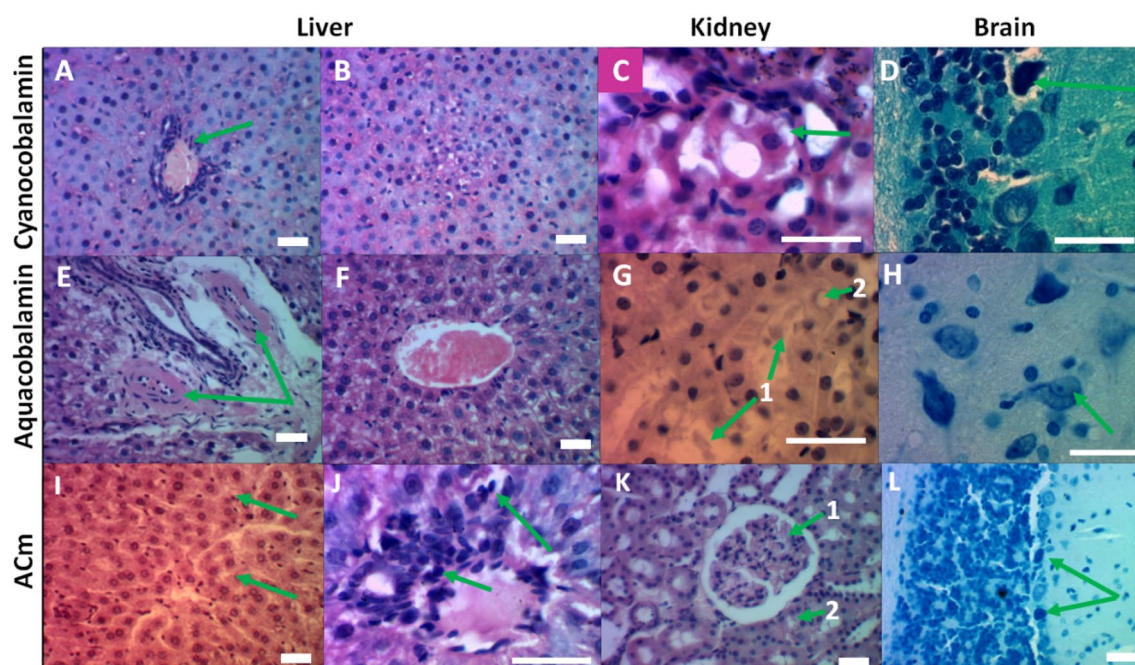


Fig. 6 Histological analysis of the studied compounds against IZ intoxication: VB12 (A–D), AQ (E–H), and ACm (I–L). Staining with hematoxylin and eosin (A, B, C, E, F, I, J, K), PAS-reaction (G), Nissl toluidine blue (D, H, L). Magnification $\times 480$ (A, B, E, F, I, K, L) and $\times 1200$ (C, D, G, H, J); scale bar corresponds to 100 μ m. **A** Congestion of the portal vein, inflammatory infiltrate with single eosinophils. **B** Vacuolar dystrophy of hepatocytes in the center of the hepatic lobule. **C** Vacuolar degeneration of nephrocytes of the proximal convoluted tubule. **D** Hyperchromia, wrinkling of the pyriform neuron of the cerebellum. **E** Spastic state of the hepatic artery

branches against the background of mild inflammatory infiltration of the portal tract stroma. **F** Plethora of the central vein, vacuolar degeneration of hepatocytes in the center of the lobule. **G** In the lumen of the distal convoluted tubules, insoluble homogeneous masses (1), focal vacuolar degeneration of nephrocytes (2). **H** Swelling of the pyramidal neuron with vacuolization of the cytoplasm. **I** Focal vacuolar degeneration of hepatocytes. **J** Single eosinophils in the composition of the inflammatory infiltrate. **K** Functional plethora of the glomerulus (1), focal degeneration of nephrocytes (2). **L** Pycnosis, hyperchromia of pear-shaped neurons of the cerebellum

the central zone of the hepatic lobules and was expressed as vacuolar degeneration (Fig. 6B) and diffuse focal intracellular cholestasis. In the cortical substance of the kidneys, acute venous plethora was noted, vacuolar degeneration of nephrocytes of the proximal convoluted tubules was focal in nature (Fig. 6C). In the brain of animals of this group, the arteries were in a state of moderately pronounced spasm,

venous plethora persists against the background of perivascular edema of the nervous tissue. Single pyramidal and pear-shaped neurons were noted in the state of pycnosis, while the nuclei and organelles of the cytoplasm were preserved (Fig. 6D). The integral expert score of histological damage was 3.2 ± 1.5 for IZ model and 2.3 ± 1.0 for VB12 which was borderline significant ($P = 0.056$).

AQ (group 4): in most cases, plethora of central veins and sinusoids of the precentral zone of the liver was noted, while in two cases, spasm of the hepatic arteries was noted (Fig. 6E). Vacuole degeneration of hepatocytes in the centers of the hepatic lobules was subtotal (Fig. 6F). The severity of the stromal inflammatory infiltrate was relatively low. In the kidneys, there was a moderately pronounced plethora of the cortical and medulla. In the lumens of the convoluted tubules, PAS-negative masses were determined while vacuolar degeneration of nephrocytes was focal (Fig. 6G). In the brain, against the background of hemostasis in the microcirculatory bed, a moderately pronounced perivascular edema of the nervous tissue was observed. Neuronal injuries differed from other groups and were characterized by focal swelling with cytoplasmic vacuolization (Fig. 6H). The integral expert score of histological damage for AQ was 2.4 ± 1.1 ($P = 0.058$).

In the case of ACm (group 5), in liver, the blood filling of all parts of the vascular bed was in most of samples. Degeneration of a few hepatocytes was noted, and, in general, the histoarchitectonics of the hepatic lobule was not disturbed (Fig. 6I). Lymphohistiocytic infiltration of the stroma in the portal tracts was mild, with only single eosinophils in its composition (Fig. 6J). The cortical substance of the kidneys had normal blood supply; vacuolar degeneration was seen only in single nephrocytes (Fig. 6K). In some samples, the lumens of the distal tubules were obturated with insoluble homogeneous masses. In the brain, signs of moderately pronounced plethora, edema of the nervous tissue, focal damage to the neurons of the cortex and cerebellum by the type of hyperchromia and pycnosis remained (Fig. 6L). The integral expert score of histological damage for ACm was 2.0 ± 1.4 ($P < 0.05$).

Thus, these VB12 compounds minimized the level of damage to hepatocytes and the severity of inflammatory cell infiltration. The corrin substances studied prevented the development of acute ischemia of the renal cortex, reduced the level of nephrocyte dystrophy, although they did not contribute to maintaining the normal functioning of the glomerular filter (especially ACm). The level of structural brain damage associated with the use of IZ remained the same for all substances studied. In the AQ group, the nature of neuronal damage was characterized by swelling of nerve cells, while pycnotic changes predominated in other groups. According to histological data, the most pronounced hepatoprotective effect was observed for ACm.

Conclusion

This study provides the first data on the antidote effect of a semi-synthetic derivative of VB12 (ACm) compared with VB12 and AQ in relation to IZ, an anti-tuberculosis drug

used in first-line therapy. In vitro experiments showed that both protonated and deprotonated forms of IZ can react with ACm. Deprotonation of IZ can lead to an increase in the reduction rate of ACm, which is the oxidizing agent of IZ in aqueous solution at various pH values. Analysis of the kinetic data showed that oxidation proceeds through complexation between ACm and IZ. This is followed by a rapid electron transfer within the corrin core to produce the reduced form of ACm and a hydrazyl radical, which further transforms into end non-toxic products. It is assumed that ACm reduces the formation of toxic metabolites from IZ oxidation.

In vivo experiments revealed that acute IZ intoxication in rats resulted in elevated levels of AST and of direct bilirubin, with a decrease in total protein levels in the blood. Damage to the liver, kidneys, and brain were confirmed histologically. Antidote usage of VB12 and ACm, which is currently not included in the official list of biologically active derivatives of VB12, contributed to the normalization of AST levels, of AQ and ACm—to the normalization of total protein in the blood serum. ACm, in addition to normalizing the levels of protein and AST, also appears to normalize the level of bilirubin in the blood. All studied compounds significantly reduced LPO. A more pronounced decrease in the values of S and S₁max in LPO was noted for ACm compared with VB12. Histological analysis confirmed the protective effects of the substances studied not only on the liver tissue, but also on the kidneys and brain. The use of all compounds minimized the level of damage to hepatocytes and the severity of inflammatory cell infiltration, prevented the development of acute ischemia in the renal cortex, and reduced the degeneration of nephrocytes and neurons. According to histology, the most pronounced hepatoprotective effect was observed for ACm.

The results suggest that ACm can serve as an antidote for IZ poisoning. A direct reaction of the compound with a toxicant is possible, leading to the formation of low-toxic derivatives. A more pronounced effect on hepatoprotection of ACm can also be explained by the fact that hydrophobic substances are better accumulated in the liver than hydrophilic ones (VB12 and AQ). In addition, in contrast to the data on ACm obtained in the first part of this work, VB12 and AQ are not able to oxidize IZ (Petrova et al. 2014), but AQ can bind it (Gromova et al. 2022). VB12 does not react with IZ. The positive effect of VB12 and its aqueous form is explained by the fact that they have a high biological activity, enhance tissue regeneration, including higher liver function. The results obtained in this work showed the feasibility of further study of VB12 and its derivatives, with special attention to its semi-synthetic hydrophobic derivatives. The conducted study indicates the prospect of correcting vitamin therapy by adding VB12 to isoniazid pharmacotherapy in patients diagnosed with tuberculosis.

Acknowledgements The authors thank Dr. Ilia Derevenkov for useful discussions.

Author contributions All authors equally contributed to this work. Unfortunately, Oscar I. Koifman passed away on 31/12/2023.

Funding There was no funding obtained for this study.

Data availability There are no new datasets generated in this manuscript. Data are available upon reasonable request.

Code availability Not applicable.

Declarations

Conflict of interest The authors declare no conflict of interest.

Ethical approval Not applicable.

Consent for publication Not applicable.

Consent to participate Not applicable.

References

- Ariga K, Mori T, Nakanishi W, Hill JP (2017) Solid surface vs liquid surface: nanoarchitectonics, molecular machines, and DNA origami. *Phys Chem Chem Phys* 19:23658–23676. <https://doi.org/10.1039/C7CP02280H>
- Ariga K, Nishikawa M, Mori T, Takeya J, Shrestha LK, Hill JP (2019) Self-assembly as a key player for materials nanoarchitectonics. *Sci Technol Adv Mater* 20:51–95. <https://doi.org/10.1080/14686996.2018.1553108>
- Ariga K, Tsai KC, Shrestha LK, Hsu SH (2021) Life science nanoarchitectonics at interfaces. *Mater Chem Front* 5:1018–1032. <https://doi.org/10.1039/D0QM00615G>
- ASPCA Animal Poison Control Center Phone Number: (888) 426–4435, <https://www.aspcapro.org/topics-animal-health/toxicology-poison-control>, Accessed 26 May 2022.
- Badrinath M, John S. Isoniazid Toxicity. 2022 Jun 27. In: StatPearls [Internet]. Treasure Island (FL): StatPearls Publishing; 2022 Jan–. PMID: 30285383, Bookshelf ID: [NBK531488](https://www.ncbi.nlm.nih.gov/books/NBK531488). <https://www.ncbi.nlm.nih.gov/books/NBK531488>
- Brenner W, Ronson TK, Nitschke JR (2017) Separation and selective formation of fullerene adducts within an MII 8L6 cage. *J Am Chem Soc* 139:75–78. <https://doi.org/10.1021/jacs.6b11523>
- Brown MJ, Symonowicz C, Medina LV, Bratcher NA, Buckmaster CA, Klein H, Anderson LC (2017) Culture of care: organizational responsibilities. *Management of animal care and use programs in research, education, and testing*, 11–26.
- Couto M, Cates C (2019) Laboratory guidelines for animal care. *Vertebrate embryogenesis*. Humana, New York, NY, pp 407–430. https://doi.org/10.1007/978-1-4939-9009-2_25
- Dale WE, Haluska GJ, Horne D (2018) Program documentation and monitoring. In: Weichbrod RH, Thompson GA, Norton JN (eds) *Management of animal care and use programs in research, education, and testing*, 2nd edn. CRC Press/Taylor & Francis, Boca Raton (FL). <https://doi.org/10.1201/9781315152189> (Chapter 15. PMID: 29787191)
- de Moraes Profirio D, Pessine FBT (2018) Formulation of functionalized PLGA nanoparticles with folic acid-conjugated chitosan for carboplatin encapsulation. *Eur Polym J* 108:311–321. <https://doi.org/10.1016/j.eurpolymj.2018.09.011>
- Edgar A, Koh M, Patel R (2022) A case of accidental isoniazid overdose presenting with nonspecific symptoms. *Cureus*. <https://doi.org/10.7759/cureus.23218>
- Erwin ER, Addison AP, John SF, Olaleye OA, Rosell RC (2019) Pharmacokinetics of isoniazid: the good, the bad, and the alternatives. *Tuberculosis* 116:S66–S70. <https://doi.org/10.1016/j.tube.2019.04.012>
- Gebremicael G, Alemayehu M, Sileshi M, Geto Z, Gebreegziabxier A, Tefera H, Desta K (2019) The serum concentration of vitamin B12 as a biomarker of therapeutic response in tuberculosis patients with and without human immunodeficiency virus (HIV) infection. *Int J Gen Med* 12:353–361. <https://doi.org/10.2147/IJGM.S218799>
- Gomes J, Durães D, Sousa A, Afonso H (2019) Isoniazid-induced acute psychosis in a patient with pleural tuberculosis. *Case Rep Psychiatry*. <https://doi.org/10.1155/2019/4272941>
- Gromova OA, Torshin IY, Maiorova LA, Koifman OI, Salnikov DS (2021) Bioinformatic and chemoneurocytological analysis of the pharmacological properties of vitamin B12 and some of its derivatives. *J Porphyrins Phthalocyanines* 25(09):835–842. <https://doi.org/10.1142/S1088424621500644>
- Gromova OA, Maiorova LA, Salnikov DS, Demidov VI, Kalacheva AG, Torshin IY, Koifman OI (2022) Vitamin B₁₂ hydrophobic derivative exhibits bioactivity: biomedical and photophysical study. *BioNanoScience* 12(1):74–82. <https://doi.org/10.1007/s12668-021-00916-4>
- Guéant JL, Guéant-Rodriguez RM, Oussalah A, Ziuly S, Rosenberg I (2023) Hyperhomocysteinemia in cardiovascular diseases: revisiting observational studies and clinical trials. *Thromb Haemost* 123:270–282. <https://doi.org/10.1055/a-1952-1946>
- Haloul M, Vinjamuri SJ, Naquiallah D, Mirza MI, Maryam Q, Chandra H, Abeer MM (2020) Hyperhomocysteinemia and low folate and vitamin B12 are associated with vascular dysfunction and impaired nitric oxide sensitivity in morbidly obese patients. *Nutrients* 12:2014. <https://doi.org/10.3390/nu12072014>
- Hendry-Hofer TB, Ng PC, McGrath AM, Soules K, Mukai DS, Chan A, Bebartha VS (2021) Intramuscular cobinamide as an antidote to methyl mercaptan poisoning. *Inhal Toxicol* 33(1):25–32. <https://doi.org/10.1080/08958378.2020.1866123>
- Jiang J, Chan A, Ali S, Saha A, Haushalter KJ, Lam WLM, Boss GR (2016) Hydrogen sulfide—mechanisms of toxicity and development of an antidote. *Sci Rep* 6(1):1–10. <https://doi.org/10.1038/srep20831>
- Kharitonova NV, Maiorova LA, Koifman OI (2018) Aggregation behavior of unsubstituted magnesium porphyrine in monolayers at air–water interface and in Langmuir-Schaefer films. *J Porphyr Phthalocyanines* 22:509–520. <https://doi.org/10.1142/S1088424618500505>
- Lee J, Mahon SB, Mukai D, Burney T, Katebian BS, Chan A, Brenner M (2016) The vitamin B12 analogcobinamide is an effective antidote for oral cyanide poisoning. *J Med Toxicol* 12(4):370–379. <https://doi.org/10.1007/s13181-016-0566-4>
- Levy J, Rodriguez-Guéant RM, Oussalah A, Jeannesson E, Wahl D, Ziuly S, Guéant JL (2021) Cardiovascular manifestations of intermediate and major hyperhomocysteinemia due to vitamin B12 and folate deficiency and/or inherited disorders of one-carbon metabolism: a 3.5-year retrospective cross-sectional study of consecutive patients. *Am J Clin Nutr*. 113:1157–1167. <https://doi.org/10.1093/ajcn/nqaa432>
- Maiorova LA, Koifman OI, Burmistrov VA, Kuvshinova SA, Mamontov AO (2015) 2D M-nanoaggregates in Langmuir layers of calamine mesogen. *Prot Metals and Phys Chem Surf* 51(1):85–92. <https://doi.org/10.1134/S2070205115010074>
- Maiorova LA, Kobayashi N, Zyablov SV, Bykov VA, Nesterov SI, Kozlov AV, Koifman OI (2018) Magnesium porphine supermolecules and two-dimensional nanoaggregates formed using the

- Langmuir-Schaefer technique. *Langmuir* 34:9322–9329. <https://doi.org/10.1021/acs.langmuir.8b00905>
- Maierova LA, Kobayashi N, Salnikov DS, Kuzmin SM, Basova TV, Koifman OI, Yang P (2023) Supramolecular nanoentities of vitamin B 12 derivative as a link in the evolution of the parent molecules during self-assembly at the air–water interface. *Langmuir* 39:3246–3254. <https://doi.org/10.1021/acs.langmuir.2c02964>
- Maierova LA, Gromova OA, Torshin IYu, Bukreeva TV, Pallaeva TN, Nabatov BV, Yabbarov NG (2024) Nanoparticles of nucleotide-free analogue of vitamin B12 formed in protein nanocarriers and their neuroprotective activity in vivo. *Colloids Surf B Biointerfaces* 244:114165. <https://doi.org/10.1016/j.colsurfb.2024.114165>
- Martin SJ, Prince SE (2017) Comparative modulation of levels of oxidative stress in the liver of anti-tuberculosis drug treated wistar rats by vitamin B12, beta-carotene, and spirulina fusiformis: role of NF- κ B, iNOS, IL-6, and IL-10. *J Cell Biochem* 118:3825–3833. <https://doi.org/10.1002/jcb.26032>
- Morris AL, Mohiuddin SS. Biochemistry, nutrients. 2022 May 8. In: StatPearls [Internet]. Treasure Island (FL): StatPearls Publishing; 2022 Jan–. PMID: 32119432, <https://www.ncbi.nlm.nih.gov/books/NBK554545>
- Nowak M, Brown TD, Graham A, Helgeson ME, Mitragotri S (2020) Size, shape, and flexibility influence nanoparticle transport across brain endothelium under flow. *Bioeng Transl Med* 5:e10153. <https://doi.org/10.1002/btm2.10153>
- O'Connor C, Brady MF. Isoniazid 2022 Apr 8. In: StatPearls [Internet]. Treasure Island (FL): StatPearls Publishing; 2022 Jan. PMID: 32491549. <https://www.ncbi.nlm.nih.gov/books/NBK557617>
- Oh C, Keats EC, Bhutta ZA (2020) Vitamin and mineral supplementation during pregnancy on maternal, birth, child health and development outcomes in low- and middle-income countries: a systematic review and meta-analysis. *Nutrients* 12(2):491. <https://doi.org/10.3390/nu12020491>. (PMID:32075071;PMCID:PMC7071347)
- Oldacre AN, Friedman AE, Cook TR (2017) A self-assembled cofacial cobalt porphyrin prism for oxygen reduction catalysis. *J Am Chem Soc* 139:1424–1427. <https://doi.org/10.1021/jacs.6b12404>
- Orssaud C, Nguyen DT, Rouzaud C, Pavie J, Pinot J, Lortholary O, Robert MP (2022) Dépistage et prévention des neuropathies optiques toxiques aux anti-mycobactériens: proposition de recommandations. *J Français d'ophtalmologie* 45(5):495–503. <https://doi.org/10.1016/j.jfo.2021.08.016>
- Ouyang M, Du Y, Meng F, Zhang X, Zhuang Q, Ma Y, Liu H, Pang M, Cai T, Cai Y (2019) Polymer-lipid hybrid nanoparticles: a novel drug delivery system for enhancing the activity of Psoralen against breast cancer. *Int J Pharm* 561:274–282. <https://doi.org/10.1016/j.ijpharm.2019.03.006>
- Petrova MV, Maierova LA, Bulkina TA, Ageeva TA, Koifman OI, Gromova OA (2014) Nanostructure of zinc(II) tetraphenylporphyrinate Langmuir M-monolayers formed with diluted solution. *Macromolecules* 47(3):267–271. <https://doi.org/10.1021/ma401116m>
- Philippopoulos GP, Tat J, Chan A, Jiang J, Mukai D, Burney T, Boss GR (2022) Methyl mercaptan gas: mechanisms of toxicity and demonstration of the effectiveness of cobinamide as an antidote in mice and rabbits. *Clin Toxicol* 60(5):615–622. <https://doi.org/10.1080/15563650.2021.2017949>
- Shee NK, Kim MK, Kim HJ (2020) Supramolecular porphyrin nanostructures based on coordination-driven self-assembly and their visible light catalytic degradation of methylene blue dye. *Nanomaterials* 10:2314–2329. <https://doi.org/10.3390/nano10112314>
- Soares S, Sousa J, Pais A, Vitorino C (2018) Nanomedicine: principles, properties, and regulatory issues. *Front Chem* 6:360. <https://doi.org/10.3389/fchem.2018.00360>
- Sridhar A, Sandeep Y, Krishnakishore C, Sriramnaveen P, Manjusha Y, Sivakumar V (2012) Fatal poisoning by isoniazid and rifampicin. *Indian Nephrol* 22(5):385. <https://doi.org/10.4103/0971-4065.103930>
- Stulz E (2017) Nanoarchitectonics with porphyrin functionalized DNA. *Acc Chem Res* 50:823–831. <https://doi.org/10.1021/acs.accounts.6b00583>
- Tumakov SO, Dereven'kov IA, Sal'nikov DS, Makarov SV (2019) Kinetics of the reaction between cobinamide and isoniazid in aqueous solutions. *Russ J Phys Chem A* 93(2):265–270. <https://doi.org/10.1134/S0036024419020274>
- Valkova LA, Shabyshev LS, Feigin LA, Akopova OB (1996a) Formation and X-ray diffraction investigation of Langmuir-Blodgett films of liquid crystalline substituted crown esters. *Mol Cryst Liq Cryst Sci Technol* 6:291–298
- Valkova L, Betrencourt C, Hochapfel A, Myagkov IV, Feigin LA (1996b) Monolayer study of monensin and lasalocid in the gas state. *Mol Cryst Liq Cryst Sci Technol A Mol Cryst Liq Cryst* 287:269–273. <https://doi.org/10.1080/10587259608038763>
- Valkova LA, Shabyshev LS, Feigin LA, Akopova OB (1997) Preparation and X-ray study of Langmuir-Blodgett films of liquid crystal 4,5'-bis(4-decyloxybenzoyloxybenzylidenamino) dibenzo-18-crown-6. *Izv Akad Nauk, Ser Fiz* 61:631–636 (WOS: A1997WZ50000048)
- Valkova LA, Shabyshev LS, Borovkov NYu, Feigin LA, Rustichelli F (1999) Supramolecular assembly formation in monolayers of tert-butyl substituted copper phthalocyanine and tetrabenzotriazaporphin. *J Incl Phenom Macrocycl Chem* 35:243–249. <https://doi.org/10.1023/A:1008147031935>
- Valkova L, Borovkov N, Maccioni E, Pisani M, Rustichelli F, Erokhin V, Nicolini C (2002) Influence of molecular and supramolecular factors on sensor properties of Langmuir-Blodgett films of tert-butyl-substituted copper azaporphyrins towards hydrocarbons. *Colloids Surf A Physicochem Eng Asp* 198–200:891–896. [https://doi.org/10.1016/S0927-7757\(01\)01016-0](https://doi.org/10.1016/S0927-7757(01)01016-0)
- Vilchèze C, Jacobs WR Jr (2019) The isoniazid paradigm of killing, resistance, and persistence in mycobacterium tuberculosis. *J Mol Biol* 431(18):3450–3461. <https://doi.org/10.1016/j.jmb.2019.02.016>
- Villar D, Knight MK, Holding J, Barret GH, Buck WB (1995) Treatment of acute isoniazid overdose in dogs. *Vet Hum Toxicol* 37(5):473–477
- Vu TT, Maierova LA, Berezin DB, Koifman OI (2016) Formation and study of nanostructured M-monolayers and LS-films of triphenylcorrole. *Macromolecules* 49:73–79. <https://doi.org/10.1021/acs.macromol.5b01105>
- Wang J, Zhou Y, Zhao C, Xiong K, Liu Y, Zhao S, Ma A (2024) Dietary patterns and the risk of tuberculosis-drug-induced liver injury: a cohort study. *Front Nutr* 11:1393523. <https://doi.org/10.3389/fnut.2024.1393523>
- Webre WA, Gobeze HB, Shao S, Karr PA, Ariga K, Hill JP, D'Souza F (2018) Fluoride-ion binding promoted photoinduced charge separation in a self-assembled C60 alkyl cation bound bis-crown etheroporphyrinogen supramolecule. *Chem Commun* 54:1351–1354. <https://doi.org/10.1039/C7CC09524D>
- Xia XS, Li X, Wang L, Wang J-Z, Ma J-P, Wu C-J (2014) Supplementation of folic acid and vitamin B12 reduces plasma levels of asymmetric dimethylarginine in patients with acute ischemic stroke. *J Clin Neurosci* 21:1586–1590. <https://doi.org/10.1016/j.jocn.2013.11.043>
- Zeytunluoglu A, Arslan I (2022) Current perspectives on nanoemulsions in targeted drug delivery, In: Handbook of research on nanoemulsion applications in agriculture, food, health, and biomedical sciences 118–140, <https://doi.org/10.4018/978-1-7998-8378-4.ch006>.
- Zhang K, Zhu S, Li J, Jiang T, Feng L, Pei J, Liu B (2021) Targeting autophagy using small-molecule compounds to improve potential








therapy of Parkinson's disease. *Acta Pharm Sin B* 11(10):3015–3034. <https://doi.org/10.1016/j.apsb.2021.02.016>

Zhang T-P, Li R, Wang L-J, Tang F, Li H-M (2022) Clinical relevance of vitamin B12 level and vitamin B12 metabolic gene variation in pulmonary tuberculosis. *Fron Immunol* 13:947897. <https://doi.org/10.3389/fimmu.2022.947897>

Publisher's Note Springer Nature remains neutral with regard to jurisdictional claims in published maps and institutional affiliations.

Springer Nature or its licensor (e.g. a society or other partner) holds exclusive rights to this article under a publishing agreement with the author(s) or other rightsholder(s); author self-archiving of the accepted manuscript version of this article is solely governed by the terms of such publishing agreement and applicable law.

Authors and Affiliations

Olga A. Gromova¹  · Larissa A. Maiorova¹  · Denis S. Salnikov²  · Ivan Yu Torshin¹  · Vadim I. Demidov³ · Irina K. Tomilova³ · O. I. Koifman² · Alla G. Kalacheva³ · Tatiana E. Bogacheva³ · Elena L. Alexakhina³ · Tatiana R. Grishina³ · Andrei N. Gromov¹ · Elham Assadpour^{4,5}  · Tolulope J. Ashaolu^{6,7}  · Seid Mahdi Jafari^{8,9} 

✉ Olga A. Gromova
unesco.gromova@gmail.com

✉ Larissa A. Maiorova
maiorova.larissa@gmail.com

✉ Seid Mahdi Jafari
smjafari@gau.ac.ir

Denis S. Salnikov
dental82@mail.ru

Ivan Yu Torshin
tiy135@yahoo.com

Vadim I. Demidov
13vid@mail.ru

Irina K. Tomilova
tomilovaivanovo@mail.ru

Alla G. Kalacheva
alla_kalacheva@mail.ru

Tatiana E. Bogacheva
tatiana.boga4iova@yandex.ru

Elena L. Alexakhina
alexakhina2013@yandex.ru

Tatiana R. Grishina
farma37@bk.ru

Andrei N. Gromov
gromlogin@gmail.com

Elham Assadpour
assadpour1170@gmail.com

Tolulope J. Ashaolu
tolulopejoshuaashaolu@duytan.edu.vn

¹ Federal Research Center “Computer Science and Control” of Russian Academy of Sciences, Moscow, Russia

² Institute of Macrocyclic Compounds, Ivanovo State University of Chemistry and Technology, Ivanovo, Russia

³ Ivanovo State Medical University, Ministry of Health of Russia, Ivanovo, Russia

⁴ Food Industry Research Co., Gorgan, Iran

⁵ Food and Bio-Nanotech International Research Center (Fabiano), Gorgan University of Agricultural Sciences and Natural Resources, Gorgan, Iran

⁶ Institute for Global Health Innovations, Duy Tan University, Da Nang 55000, Viet Nam

⁷ Faculty of Medicine, Duy Tan University, Da Nang 55000, Viet Nam

⁸ Department of Food Materials and Process Design Engineering, Gorgan University of Agricultural Sciences and Natural Resources, Gorgan, Iran

⁹ Iran Food and Drug Administration, Halal Research Center of IRI, Ministry of Health and Medical Education, Tehran, Iran